# Electrically Tunable Reactivity of Substrate-Supported Cobalt Oxide Nanocrystals

*Ana Sánchez-Grande, Huu Chuong Nguyën, Koen Lauwaet, Jonathan Rodríguez-Fernández,* Esther Carrasco, Borja Cirera, Zhaozong Sun, José Ignacio Urgel, Rodolfo Miranda, Jeppe V. Lauritsen, José M. Gallego,* Nuria López,* and David Écija**

**First-row transition metal oxides are promising materials for catalyzing the oxygen evolution reaction. Surface sensitive techniques provide a unique perspective allowing the study of the structure, adsorption sites, and reactivity of catalysts at the atomic scale, which furnishes rationalization and improves the design of highly efficient catalytic materials. Here, a scanning probe microscopy study complemented by density functional theory on the structural and electronic properties of CoO nanoislands grown on Au(111) is reported. Two distinct phases are observed: The most extended displays a Moiré pattern ($\alpha$-region), while the less abundant is 1Co:1Au coincidental ($\beta$-region). As a result of the surface registry, in the $\beta$-region the oxide adlayer is compressed by 9%, increasing the unoccupied local density of states and enhancing the selective water adsorption at low temperature through a cobalt inversion mechanism. Tip-induced voltage pulses irreversibly transform $\alpha$- into $\beta$-regions, thus opening avenues to modify the structure and reactivity of transition metal oxides by external stimuli like electric fields.**

## 1. Introduction

The depletion of fossil fuels combined with the growing energy consumption and the need for environmental protection urges us to find renewable energy solutions.[1] Photoelectrocatalytic cells (PEC), which transform $H_2O$ and $CO_2$ into oxygen and solar fuels using the sun energy, have emerged as a promising alternative.[2,3] The bottleneck for PEC efficiency is the oxygen evolution reaction (OER),[4,5] in which water oxidation produces oxygen at the anode. Oxides of transition metals (TMOs), such as $IrO_x$[6,7] and $RuO_2$,[8,9] are good candidates for catalyzing the OER, but they are scarce and expensive. Therefore, there is a need for the development of OER catalysts formed by earth-abundant and environmentally friendly materials. Promising candidates are TMOs based on first-row transition metals, like Ni, Co, and Fe.[10,11]

These first-row transition metals present multivalent oxidation state that enhances their versatility and allows to modify the structure, electronic properties and phase diagram by external stimuli.[12,13] However, as materials reconstruct in the presence of potential, solvent and electrolytes revealing the intrinsic relationships between as-prepared materials, the true structure under reaction conditions and the electrochemical response remains the hugest rational gap in the field. Correlations have been established between the native (as prepared) materials and activity but the dynamics induced by the environment, reaction, and external stimuli might be crucial and the lack of robust structure-activity relationships is limiting our understanding and further optimization. Atomistic insights, providing further understanding of the water splitting process,[14–16] have been obtained for various TMOs, such as $Fe_3O_4$,[17,18] $\alpha$-$Fe_2O_3$,[19] NiO,[20,21] $TiO_2$,[22] CoO,[23] and $Co_2O_3$,[23] by means of scanning probe microscopy and other surface techniques, but usually in steady state. Up to now, atomistic studies of the tunability of the physico–chemical properties of substrate-supported TMOs by modifying their crystallographic relationship with the substrate, using for example the atom manipulation capabilities of a scanning probe, have remained elusive.

The investigation of the nature of the structure and chemical composition of these oxides is fundamental to obtain robust

A. Sánchez-Grande, K. Lauwaet, E. Carrasco, B. Cirera, J. I. Urgel, R. Miranda, D. Écija
IMDEA Nanociencia.
Madrid 28049, Spain
E-mail: david.ecija@imdea.org
H.C. Nguyën, N. López
Institute of Chemical Research of Catalonia (ICIQ)
The Barcelona Institute of Science and Technology
Tarragona 43007, Spain
E-mail: nlopez@iciq.es
J. Rodríguez-Fernández,[+] Z. Sun, J. V. Lauritsen
Interdisciplinary Nanoscience Center
Aarhus University
Aarhus C DK-8000, Denmark
E-mail: rodriguezjonathan@uniovi.es
R. Miranda
Dep. Física de la Materia Condensada
Universidad Autónoma de Madrid
Cantoblanco, Madrid 28049, Spain
J. M. Gallego
Instituto de Ciencias Materiales – CSIC
Cantoblanco, Madrid 28049, Spain
E-mail: josemaria.gallego@imdea.org
The ORCID identification number(s) for the author(s) of this article can be found under https://doi.org/10.1002/smll.202106407.
[+]Present address: Dep. de Física, Universidad de Oviedo, Oviedo 3307, Spain

structural-activity relationships that can steer synthetic efforts. The study of ultra-thin films on substrates, paying special attention to their electronic properties, can provide the fundamental knowledge of the properties of such oxide layers and their correlation with the intrinsic catalytic activity.[24]

Within the first-row TMOs, cobalt oxides are relevant due to their compositional and crystallographic phase variability.[25,26] Cobalt can be found as $Co^{2+}$ (c-CoO: rocksalt and h-CoO: wurtzite structure),[27] $Co^{3+}$ ($Co_2O_3$: corundum and $CoO_2$-$LiCoO_2$),[26,28] or a mixture of them ($Co_3O_4$: spinel structure).[29] Recently, the growth of ultra-thin nanoislands of c-CoO(111) bilayers on Au(111) has been reported, reproducing the structure of rocksalt cobalt oxide with a (111) surface termination.[30] Notably, it was shown, by means of room temperature scanning tunneling microscopy (STM), that the OER catalytic activity of CoO nanoislands on Au(111) increases for smaller island size due to the higher reactivity at the borders of the islands.[14]

Here, we report the growth of c-CoO bilayer nanoislands on Au(111) as a model system to correlate the structural and electronic properties and their interaction with the surface. To this aim, we have employed STM, scanning tunneling spectroscopy (STS), and non-contact atomic force microscopy (nc-AFM), complemented by X-ray photoelectron spectroscopy (XPS), and density functional theory (DFT). The c-CoO nanoislands present two phases: i) The more extended phase displays a Moiré pattern, with a relatively large unit cell ($\alpha$-region); ii) the minority phase is a 1Co:1Au coincidental structure, and shows an enhancement of the unoccupied density of states and an increased reactivity ($\beta$-region). Notably, voltage-induced pulses can locally and irreversibly transform the $\alpha$-regions into a $\beta$-region, thus modifying the atomic and electronic structure of CoO by external stimuli.

Nanoislands of CoO were formed on Au(111) (see **Figure 1**a) following a recently reported protocol,[23] which is based on the evaporation of cobalt onto Au(111) in an oxygen pressure (see Experimental Methods in Supporting Information for further details). The growth was monitored by XPS (as illustrated in Figure S1, Supporting Information) and STM. Under these conditions, single bilayer CoO nanoislands are formed, with a bottom layer of Co atoms and a top layer of O atoms,[30,31] reproducing the (111) surface of rocksalt structure. Sporadically, minority double bilayer nanoislands (Co—O—Co—O from

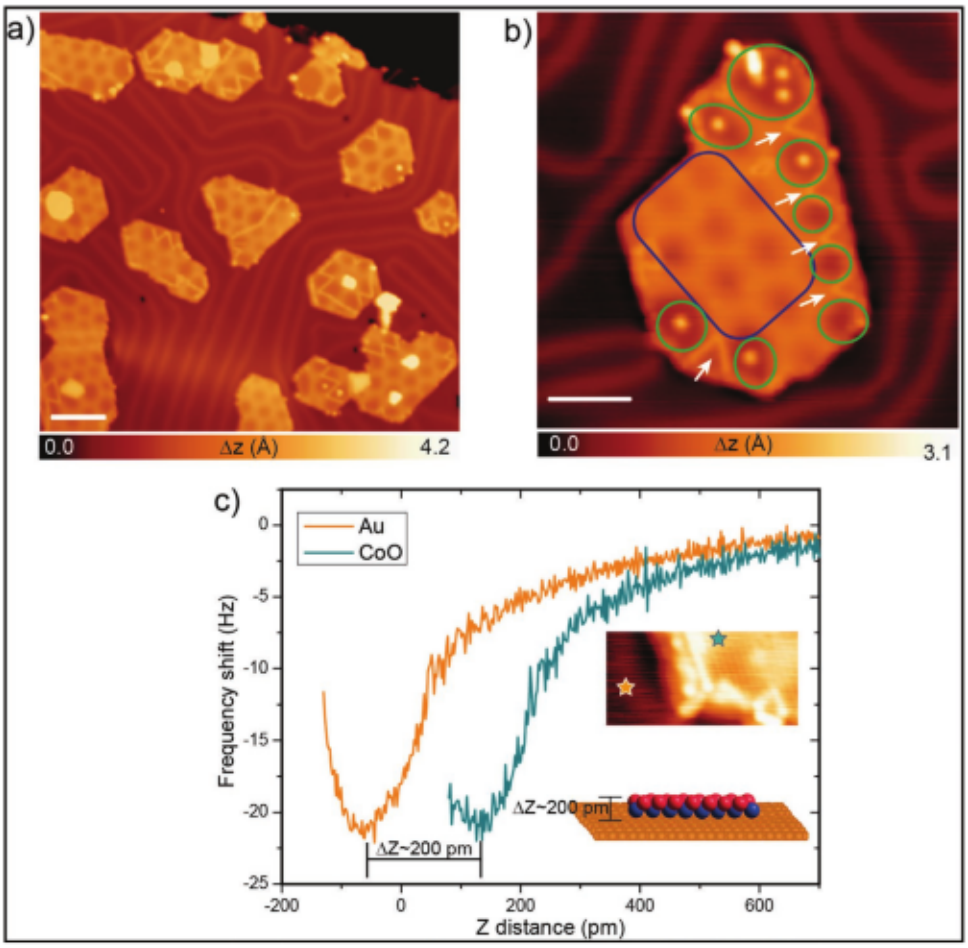


**Figure 1.** Growth of single bilayer CoO islands on Au(111). a) Constant-current STM image overview of single bilayers CoO islands with a diameter of ≈15–20 nm ($V_b = -1.0$ V, $I_t = 100$ pA, scale bar = 10 nm). b) High-resolution STM image of a CoO single bilayer island. The $\alpha$-region, marked by a blue rectangle, features a Moiré pattern. The darker areas outside the blue rectangle (highlighted with green circles) are $\beta$-regions ($V_b = -1.0$ V, $I_t = 100$ pA, scale bar = 5 nm). c) Force spectroscopy measurements taken on the Au(111) surface (orange line) and on the bright area of the Moiré pattern of the CoO island (green line), resulting in an island height of ≈200 ± 20 pm.

bottom to top) can be found, as shown in Figures S2 and S3, Supporting Information.

In this work, we have focused on the single bilayer CoO nanoislands, which is the majority product as can be seen in Figure 1a and Figure S2, Supporting Information. Such islands feature two distinct regions, to be termed $\alpha$- and $\beta$-regions, as can be seen in Figure 1b. $\alpha$-regions display a Moiré pattern because of the mismatch between the CoO and the Au111 surface (see area highlighted by a blue rectangle in Figure 1b). The average periodicity of the Moiré pattern is ≈(34 ± 2) Å for medium size islands. The double bilayer islands also display a Moiré pattern, but with a smaller periodicity =(28 ± 2 Å) (see Figure S3, Supporting Information).

$\beta$-regions (darker regions when imaged at $V_b = -1$ V and highlighted by green circles in Figure 1b) do not exhibit a Moiré pattern and are usually observed adjacent to the borders of the islands or next to oxygen adatom dislocation lines[32] (bright lines marked with white arrows in Figure 1b). The domain size of such $\beta$-regions ranges between 2 and 8 nm (Figure S4, Supporting Information). Occasionally, bright protrusions, which are assigned to adsorbates, are selectively observed on top of the $\beta$-regions, which will be discussed below. Remarkably, in standard constant-current STM images, $\beta$-regions look similar in appearance to the dark areas of the Moiré (although the dimensions of $\beta$-region are typically larger), and probably due to this similarity they have not been previously reported.

The height of the single layer CoO nanoislands cannot be reliably measured by STM due to the convolution of the topographic and electronic structure of the island while probed by the tip. This is evidenced by the change in the apparent height of the islands, between 1.3 and 1.0 Å, depending on the bias voltage (illustrated in Figure S5, Supporting Information). To circumvent such limitations in the elucidation of the topographic height of the CoO nanoislands, we have performed atomic force spectroscopy measurements, which is a technique capable of measuring the height variations of the probed samples.[33] In Figure 1c two force spectra acquired sequentially on top of a CoO island and on the adjacent Au(111) surface are shown (orange and green lines, respectively). The distance between the two frequency shift minima reveals that the height of the CoO single bilayer islands with respect to the substrate is 200 ± 20 pm, in agreement with results of 3d TMOs supported on metals, such as, FeO[34] and ZnO.[35]

**Figure 2**a shows a high resolution STM image of the $\alpha$-region, in which the average experimental interatomic distance of the CoO layer ($d_{CoO}$) is 3.3 ± 0.2 Å, as recently reported.[31] Such result is in agreement with the low energy electron diffraction (LEED) pattern displayed in Figure 2b, which shows two hexagonal lattices: in reciprocal space, the larger one corresponding to the pristine Au(111) surface and the shorter one to the CoO islands. Considering 2.88 Å the tabulated value of $d_{Au[111]}$, the relation between both lattices results in $d_{CoO}$ of 3.4 ± 0.1 Å, (significantly larger than the one determined for the $CoO_2$ (3.12 Å)),[36] corroborating the growth of CoO nanoislands. (The small differences between the results of the LEED pattern and the STM images are attributed to the contribution of second layer islands to the LEED pattern). Although the STM images show that the Moiré pattern is slightly irregular, a detailed analysis of the STM and LEED data (see discussion in Note S1, Supporting Information) suggests that the structure of CoO in an the $\alpha$-region can be approximately described with an epitaxial relationship with respect to the substrate of $\begin{pmatrix} 11 & -1 \\ 1 & 11 \end{pmatrix}$, as can be seen in the model proposed in Figure 2c. As a result, along the Moiré unit cell Co and O atoms can be found in the following adsorption registries: Co and O in threefold with respect to Au atoms, Co on top and oxygen in threefold or O on top and Co in threefold (such situations are highlighted in Figure 2c with a purple, green, and blue circle, respectively). STM simulations of the DFT relaxed configuration of this model compare favorably well with the experiment results, as can be seen in Figure 2d.

A high-resolution constant-current STM image of a nanoisland displaying both the $\alpha$- and the $\beta$-regions is shown in **Figure 3**a. Comparison of line profiles taken on both regions (Figure 3b) reveals that the $\beta$-region has a uniform interatomic distance of 3.0 ± 0.2 Å, which is smaller than the interatomic distance in the Moiré region and very close to the lattice parameter of the Au(111) surface. Thus, the $\beta$-region is assigned structurally to a compressed c-CoO (111) structure, which is 1Co:1Au coincidental with the Au(111) surface, explaining the absence of a Moiré pattern in this region.

Here it is important to note that previously, and under electrochemical conditions, a synergic catalytic effect between the Co oxide and the gold have been reported,[37,38] although no detailed model has been accepted so far to explain the nature of this enhancement. Since this hitherto unreported second phase of the oxide (the $\beta$-region), induced by the registry with the underlying substrate, might show different electronic properties of the CoO layer, it could also lead to a change in the reactivity of the oxide.

Therefore, we have performed STS on both the brighter and the darker areas of the Moiré pattern, and on the $\beta$-region (see Figure 3c,d). Although the brighter Moiré region (imaged at negative bias voltage) shows a higher occupied and a lower unoccupied local density of states (LDOS) close to Fermi level compared to the darker Moiré region (see vertical zoom-in of purple and green spectra in Figure S6, Supporting Information), tentatively suggesting charge transfer from the gold to the brighter Moiré area (also obtained in the modeling where Bader charges are larger for O-atoms closer to Au, see below). The clearest difference appears when comparing the $\alpha$-region (either bright or dark) with the $\beta$-region, the latter showing a much higher unoccupied LDOS (see gray curve in Figure 3d), which reveals that lattice parameter differences indeed have a strong impact in the electronic properties of the CoO nanoisland.

Surprisingly, while performing these measurements, we noticed that it was possible to irreversibly transform the $\alpha$-region into $\beta$-region with the STM tip. In fact, such transformation could be achieved by acquiring $I/V$ curves (Figure S7, Supporting Information) or by applying tip induced pulses with open feedback loop as shown in **Figure 4**a–d. In the latter, the transformation was induced with a voltage pulse of −8.0 V (the threshold value of voltages needed to induce the transformation depends on the tip), and was observed up to 1 nm away from the point where the voltage pulse was applied, suggesting that the process is triggered mainly by the electric field. The change from Moiré to $\beta$- structure is clearly visualized as a compression by taking comparative line profiles of the regions shown in Figure 4e, confirming an atomic compression of =9%. The reverse transformation from $\beta$-region to $\alpha$- region was never observed.

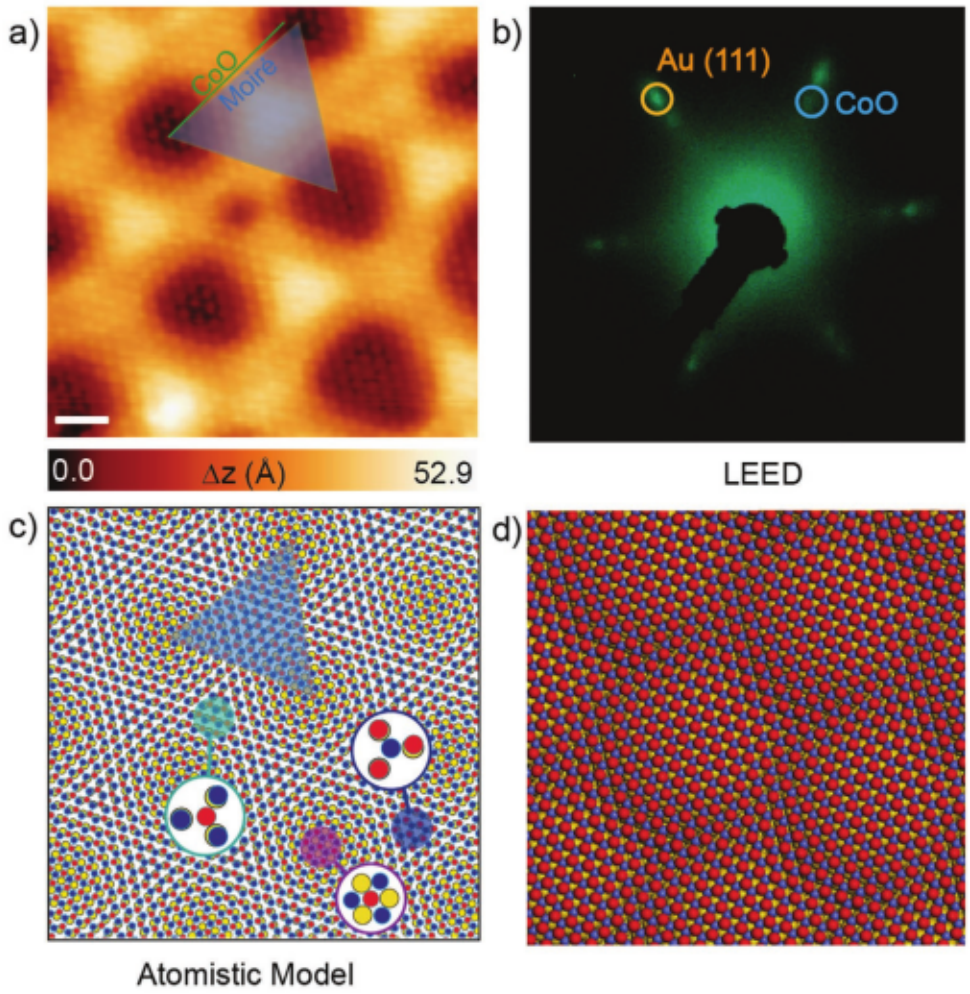


**Figure 2.** Structural insights into the $\alpha$-region of single bilayer CoO islands on Au(111). a) High-resolution STM image of a CoO single bilayer nanoisland ($V_b = -0.001$ V, $I_t = 750$ pA, scale bar = 1 nm). b) LEED image of a sample of CoO islands on Au(111), grown by the protocol reported in the main text (acquired at an energy $E_p = 58.1$ eV). Spots of the respective lattices are marked with circles. c) Atomistic model of the CoO single bilayer on Au(111). The CoO layer is slightly rotated by $\theta_{CoO\text{-}Au} = 0.5°$ with respect to the high symmetry directions of the Au(111) surface. d) DFT model of the geometry structure of the Moiré region. c,d) Yellow, red, and blue balls correspond to gold, oxygen, and cobalt atoms, respectively.

The majority of pristine CoO nanoislands consist of Moiré $\alpha$-regions, though it is observed that the $\alpha \rightarrow \beta$ transformation is irreversible. To rationalize this effect, we can tentatively deduce the following scenario: at the employed growth temperatures, the CoO nanoislands adopt a lattice parameter very similar to the ideal lattice parameter of an isolated CoO bilayer ($\alpha$-phase), giving rise to the characteristic Moiré pattern on the Au(111) surface. However, at lower temperatures, the 1Co:1Au coincidental $\beta$-region seems to be more stable (since the transformation $\alpha \rightarrow \beta$ is irreversible). As the $\alpha$-phase survives the cool down to 4 K and only minor $\beta$-regions appear (both of them measured with the STM), it follows that the transition from the $\alpha$-phase to the $\beta$-phase requires surpassing an energy barrier. Applying a voltage pulse helps to surpass this barrier, leading to the more stable $\beta$-phase. The computational modeling based on DFT supports this view. First, benchmarking the electronic structure of the standing layers demonstrates the difficulties of standard PBE in assessing the correct structure for the Moiré pattern (i.e., the free CoO and Au present the same lattice parameter, thus there is no possibility for a Moiré), see Tables S1–S3, Supporting Information. Thus, PBEsol needs to be employed, when doing so, the $\beta$- is more stable than the $\alpha$-region and according to the Bader charges (Table S4, Supporting Information), the charge transfer between the oxide layer and Au is larger in the $\beta$-region; this is supported by the larger dipole Table S5, Supporting Information.

Thus, as shown in Figure 4a–d, the $\beta$-phase is both topographically and electronically different from the Moiré region, which could lead to distinct chemical properties. In fact, and as noted in the beginning, the STM images show that the $\beta$-regions are often found decorated by some type of adsorbate, as illustrated in Figure 1b (green circle) and Figure S8, Supporting Information. Probably these adsorbates are coming from the residual gas always present in the UHV chamber. Such species are imaged as bright protrusions, and they are found exclusively on $\beta$-regions. In addition, STM tip manipulation experiments allow us to move these adsorbates within a $\beta$-region and between different $\beta$-regions, (Figure S8, Supporting Information).[39] Notably, even with tip manipulation, these molecular adsorbates never attach to the regular Moiré

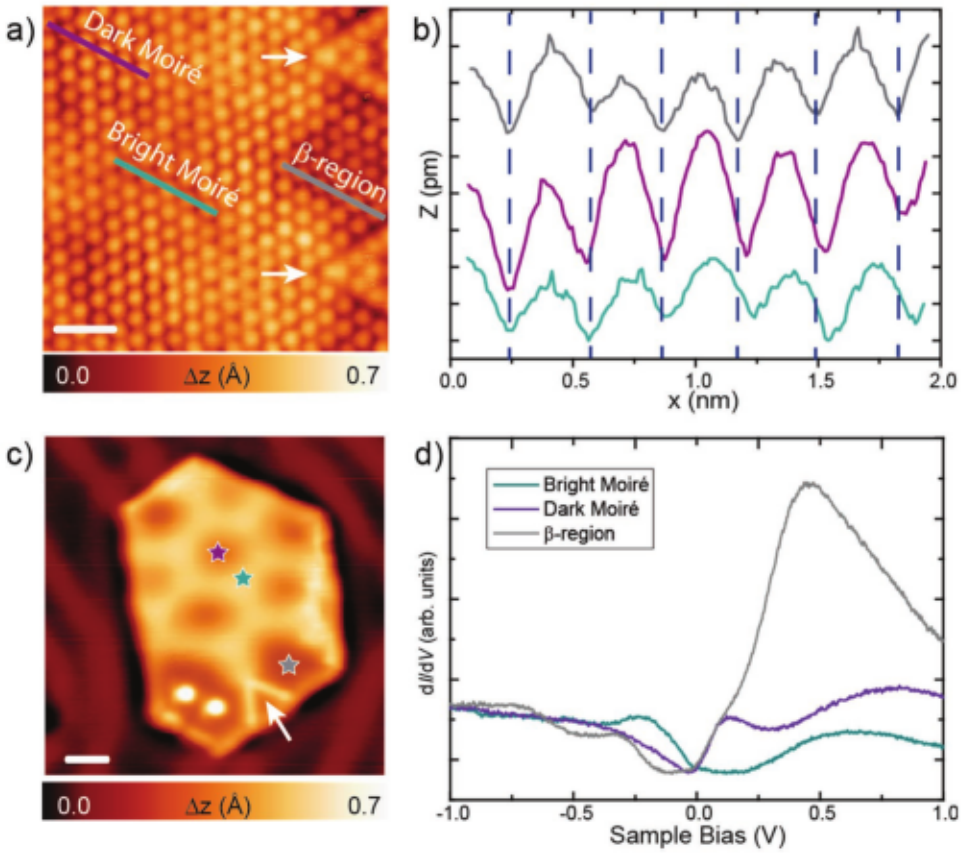


**Figure 3.** Lateral interatomic distances and electronic properties of a single bilayer CoO on Au(111). a) High-resolution STM image of the surface of a CoO nanoisland showing both $\alpha$- (the Moiré area, left side of the image) and $\beta$-regions (right side). The bright lines on the right side of the image, marked with white arrows have been interpreted as oxygen adatom dislocation lines[32] ($V_b = -0.1$ mV, $I_t = 700$ pA, scale bar = 1 nm). b) Height profiles extracted from (a), plotted in a stack form, for comparison between brighter Moiré area (green line, bottom) with the longest interatomic distance, darker Moiré area (purple line, middle) with a slightly shorter interatomic distance, and $\beta$-region (gray line, top) with the shortest interatomic distance. c) STM image of a CoO nanoisland containing both Moiré and $\beta$-region. ($V_b = -0.4$ V, $I_t = 500$ pA, scale bar = 2 nm). d) Comparison of the scanning tunneling spectra acquired at the moiré area (green and purple lines) with respect to the $\beta$-region (gray line), revealing a remarkably increase of the local density of unoccupied states in $\beta$-region. The spectra positions are depicted in (c).

area, indicating a distinct binding energy on both regions, being such adsorption more favorable on the $\beta$-regions.

To find out the nature of the adsorbate, we have intentionally dosed $H_2$ and CO to the CoO nanoislands. However, STM images in Figure S9, Supporting Information, show that in neither case it is observed an increase in the average number of adsorbates on the CoO nanoislands as compared to pristine samples. In agreement with these results, DFT shows that neither CO nor $CO_2$ adsorb effectively on the $\beta$-regions (+0.16 eV and –0.16 eV binding energy, respectively).

Since water is also a common background gas in UHV chambers, we have exposed the CoO islands at room temperature to water vapor (100 L) and subsequently cooled down the samples to 4 K before imaging them with STM (Figure S10, Supporting Information). The resulting images show the presence of bright adsorbates on the $\beta$-regions, very similar to those observed with no intentional exposure, and a number of smaller and dimmer protrusions on the surface, mainly on the Moiré areas, that are easily distinguishable from the larger brighter protrusions. Previous studies have identified the smaller adsorbates as hydroxyl groups,[14] that is, H atoms adsorbed on the O atoms of the CoO layer forming hydroxyl groups, coming from the water splitting reaction. Unlike the initial brighter adsorbates, these hydroxyl groups are present on the Moiré regions as well, leading us to exclude the hydroxyl group as a candidate. Thus, it is possible that the brighter adsorbates observed in the $\beta$-regions stem from intact water molecules being adsorbed during or after the cool down process.

In order to check this hypothesis, we modeled the water adsorption process on both regions of the CoO nanoislands. Molecular adsorption energy on the basic centers of the $\beta$-region is –0.22 eV, while on the Moiré area it is –0.27 eV. However, this energy difference will be equivalent to the entropic contribution and, thus, this physisorption cannot be responsible for the observations. First, following the reported enhanced adsorption of TMOs due to oxygen vacancies,[40] we have studied the effect of possible oxygen vacancies in the CoO layer. An oxygen vacancy leads to an increase in the adsorption energy on the $\beta$-regions to –0.67 eV. However, the STM images never revealed any indication of the possible existence of O vacancies in the oxide layer, even after removal of the water molecules by applying STM pulses (Figures S8 and S11,

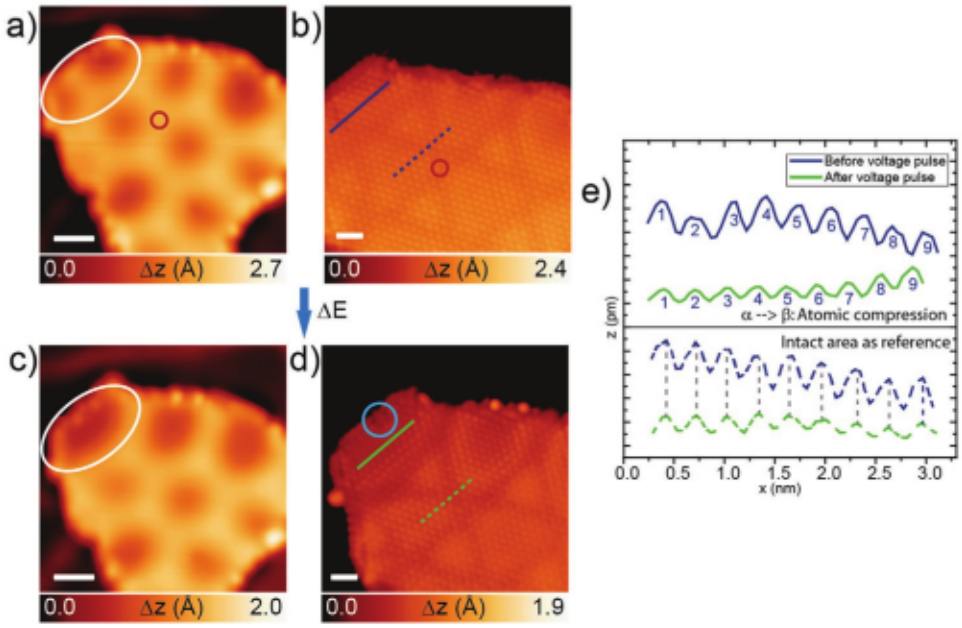


**Figure 4.** Field-induced transformation of the Moiré into the $\beta$-region within a single bilayer CoO nanoisland on Au(111). a) Constant-current STM image of a CoO single bilayer island before applying a voltage pulse ($V_b$ = 1.0 V, $I_t$ = 100 pA, scale bar = 2 nm). The red circle marks the position of the subsequent voltage tip pulse ($V_b$ = –8 V, $I_t$ = 100 pA, $t$ = 30 ms). b) STM image of the same region acquired with atomic resolution ($V_b$ = –0.02 V, $I_t$ = 700 pA, scale bar = 1 nm). c) Constant current STM image after the modification of the area. The white circle indicates the area transformed into $\beta$-region ($V_b$ = 1.0 V, $I_t$ = 100 pA, scale bar = 2 nm). d) STM image displaying atomic resolution after the bias pulse. ($V_b$ = –0.2 V, $I_t$ = 50 pA, scale bar = 1 nm). e) Full lines: Height profiles extracted from the island in the modified region before (blue lines) and after (green lines) the modification revealing the compression of the atoms. Dashed lines: Height profiles of a pristine region of the island, taken as reference, before and after the voltage pulse, showing no change in the interatomic distance.

Supporting Information), and thus discard the role of oxygen vacancies in selective water adsorption. A second hypothesis is a local atomic inversion of the oxide nanoisland, that is, under the influence of a water molecule a Co atom could diffuse up from the first Co layer in contact with the substrate to the top of the nanoisland by crossing the oxygen plane (see Figure S12, Supporting Information, for a schematic view of the proposed mechanism). The water molecule is bound to the pulled-up Co, leading to an adsorption energy of –1.05 eV in the $\beta$-regions upon distortion. The calculated energy needed to distort Co is 0.69 eV lower in the $\beta$-regions than in the Moiré area, making this process in the Moiré areas unlikely and adsorption on beta irreversible. The lower rearrangement energy in the $\beta$-region stems from the fact that here the CoO layer is compressed with respect to the ideal lattice parameter of an isolated layer, thus making easier to distort the layer by expelling out a Co atom. The combination of distortion and electron rearrangement can be interpreted as a polaron-like state.[13,41]

As mentioned before, the lattice parameter in the Moiré areas is ≈3.3 Å, which is larger than the lattice parameter in the (111) plane of bulk CoO. Since the (111) termination of CoO is a polar surface, this expansion has been explained as a way of reducing the surface dipole, as it allows the Co and O layers to move closer.[32] On the contrary, for the $\beta$-regions, with a smaller lattice parameter, the vertical distance between the layers increases, and so does the surface dipole. Actually, our simulations indicate that the $\beta$-region has a dipole moment density more than five times larger than the Moiré region (see Table S5, Supporting Information). The displacement of the Co atom reduces the magnitude of this dipole, but the decrease is much more significant after the adsorption of the water molecule (see Table S5, Supporting Information).

Altogether, we thus propose that the detected adsorbates on the $\beta$-regions stem from water molecules captured during cooldown of the sample (for instance during the pressure increase when moving the low temperature shields of the STM). These water molecules initially bind with van der Waals interactions to the islands, where they remain mobile due to the low diffusion barrier. If they adsorb on an island with $\beta$-regions, they can be captured by a local cobalt inversion, which reduces the surface dipole. On islands without $\beta$-regions they will eventually reach the borders and stick there, as the borders of the islands usually present some irregular features.

## 2. Conclusions

In summary, we report a low temperature STM and nc-AFM study, complemented by LEED and DFT simulations, of single layer CoO nanoislands and their transformations on Au(111). Two distinct topographically and electronically regions are identified within the islands: the $\alpha$- and the $\beta$-regions. Majority area is the $\alpha$-region, featuring a Moiré, with a nearest neighbor's distance of =3.3 Å and whose unit cell is rotated by 0.5° with respect to the Au(111) substrate. In the minority $\beta$-region the lattice parameter is ≈3.0 Å and in registry with the substrate. Such $\beta$-phase exhibits a larger density of unoccupied states than the $\alpha$-region. Notably, by tip-induced voltage pulses, the $\alpha$-region

can be transformed irreversibly to $\beta$-areas, which seems to more stable under the geometrical constraints imposed by the Au(111) substrate. The topographic and electronic peculiarities of the $\beta$-region result in the selective adsorption of residual water species at low temperatures as compared to the incommensurate CoO areas, possibly through the formation of polaron-like states driven by local cobalt inversion.

Our study highlights the influence of the registry of ultrathin film oxides on their structural and electronic properties, and consequently in the binding of relevant molecular species for catalysis. Furthermore, we anticipate fascinating avenues for tunable catalysts by external stimuli like electric fields.


## Acknowledgements

This work was supported by the European Union under the H2020 FET-PROACT A-LEAF (Artificial-Leaf) project (Grant Agreement No. 732840). The authors thank Prof. Aleksandra Vojvodic for helpful discussion about her previous works about the nature of CoO nanoislands on Au(111). The authors thankfully acknowledge the computer resources at MareNostrum and the technical support provided by the Barcelona Supercomputing Center (QS-2019-3-0029 Advanced atomistic simulations in (electro)-catalysis for a circular economy).


## Conflict of Interest

The authors declare no conflict of interest.

## Data Availability Statement

The data that support the findings of this study are openly available in ioChem-BD[42] at [https://doi.org/10.19061/iochem-bd-1-218].


## Keywords

cobalt, dynamic structural changes, oxide, oxygen evolution reaction, scanning tunneling microscopy



[1] Z. W. Seh, J. Kibsgaard, C. F. Dickens, I. Chorkendorff, J. K. Nørskov, T. F. Jaramillo, *Science* **2017**, *355*, 4998.

[2] B. Alfaifi, H. Ullah, S. Alfaifi, A. Tahir, T. Mallick, *Veruscript Funct. Nanomater.* **2018**, *2*, BDJOC3.

[3] J. R. Galan-Mascaros, *Catal. Sci. Technol.* **2020**, *10*, 1967.

[4] V. Viswanathan, H. A. Hansen, J. Rossmeisl, J. K. Nørskov, *ACS Catal.* **2012**, *2*, 1654.

[5] A. Vojvodic, J. K. Nørskov, *Natl. Sci. Rev.* **2015**, *2*, 140.

[6] V. Pfeifer, T. E. Jones, S. Wrabetz, C. Massué, J. J. V. Vélez, R. Arrigo, M. Scherzer, S. Piccinin, M. Hävecker, A. Knop-Gericke, R. Schlögl, *Chem. Sci.* **2016**, *7*, 6791.

[7] H. N. Nong, L. J. Falling, A. Bergmann, M. Klingenhof, H. P. Tran, C. Spöri, R. Mom, J. Timoshenko, G. Zichittella, A. Knop-Gericke, S. Piccinin, J. Pérez-Ramírez, B. Roldan-Cuenya, R. Schlögl, P. Strasser, D. Teschner, T. E. Jones, *Nature* **2020**, *587*, 408.

[8] H. Over, *Science* **2000**, *287*, 1474.

[9] R. R. Rao, M. J. Kolb, N. B. Halck, A. F. Pedersen, A. Mehta, H. You, K. A. Stoerzinger, Z. Feng, H. A. Hansen, H. Zhou, L. Giordano, J. Rossmeisl, T. Vegge, I. Chorkendorff, I. E. L. Stephens, Y. Shao-Horn, *Energy Environ. Sci.* **2017**, *10*, 2626.

[10] C. C. L. McCrory, S. Jung, J. C. Peters, T. F. Jaramillo, *J. Am. Chem. Soc.* **2013**, *135*, 16977.

[11] C. G. Morales-Guio, L. Liardet, X. Hu, *J. Am. Chem. Soc.* **2016**, *138*, 8946.

[12] C. B. Gopal, M. García-Melchor, S. C. Lee, Y. Shi, A. Shavorskiy, M. Monti, Z. Guan, R. Sinclair, H. Bluhm, A. Vojvodic, W. C. Chueh, *Nat. Commun.* **2017**, *8*, 15360.

[13] F. A. Garcés-Pineda, M. Blasco-Ahicart, D. Nieto-Castro, N. López, J. R. Galán-Mascarós, *Nat. Energy* **2019**, *4*, 519.

[14] J. Fester, M. García-Melchor, A. S. Walton, M. Bajdich, Z. Li, L. Lammich, A. Vojvodic, J. V. Lauritsen, *Nat. Commun.* **2017**, *8*, 14169.

[15] J. Fester, A. Makoveev, D. Grumelli, R. Gutzler, Z. Sun, J. Rodríguez-Fernández, K. Kern, J. V. Lauritsen, *Angew. Chem.* **2018**, *130*, 12069.

[16] Z. Jakub, J. Hulva, F. Mirabella, F. Kraushofer, M. Meier, R. Bliem, U. Diebold, G. S. Parkinson, *J. Phys. Chem. C* **2019**, *123*, 15038.

[17] B. Stanka, W. Hebenstreit, U. Diebold, S. A. Chambers, *Surf. Sci.* **2000**, *448*, 49.

[18] G. S. Parkinson, *Surf. Sci. Rep.* **2016**, *71*, 272.

[19] F. Kraushofer, Z. Jakub, M. Bichler, J. Hulva, P. Drmota, M. Weinold, M. Schmid, M. Setvin, U. Diebold, P. Blaha, G. S. Parkinson, *J. Phys. Chem. C* **2018**, *122*, 1657.

[20] A. Barbier, C. Mocuta, H. Kuhlenbeck, K. F. Peters, B. Richter, G. Renaud, *Phys. Rev. Lett.* **2000**, *84*, 2897.

[21] L. Gragnaniello, F. Allegretti, R. R. Zhan, E. Vesselli, A. Baraldi, G. Comelli, S. Surnev, F. P. Netzer, *Surf. Sci.* **2013**, *611*, 86.

[22] U. Diebold, *Surf. Sci. Rep.* **2003**, *48*, 53.

[23] J. Fester, Z. Sun, J. Rodríguez-Fernández, A. Walton, J. V. Lauritsen, *J. Phys. Chem. B* **2018**, *122*, 561.

[24] G. W. Sievers, A. W. Jensen, J. Quinson, A. Zana, F. Bizzotto, M. Oezaslan, A. Dworzak, J. J. K. Kirkensgaard, T. E. L. Smitshuysen, S. Kadkhodazadeh, M. Juelsholt, K. M. Ø. Jensen, K. Anklam, H. Wan, J. Schäfer, K. Čépe, M. Escudero-Escribano, J. Rossmeisl, A. Quade, V. Brüser, M. Arenz, *Nat. Mater.* **2021**, *20*, 208.

[25] S. G. Kandalkar, J. L. Gunjakar, C. D. Lokhande, *Appl. Surf. Sci.* **2008**, *254*, 5540.

[26] F.-C. Kong, Y.-F. Li, C. Shang, Z.-P. Liu, *J. Phys. Chem. C* **2019**, *123*, 17539.

[27] W. Meyer, D. Hock, K. Biedermann, M. Gubo, S. Müller, L. Hammer, K. Heinz, *Phys. Rev. Lett.* **2008**, *101*, 016103.

[28] T. Motohashi, Y. Katsumata, T. Ono, R. Kanno, M. Karppinen, H. Yamauchi, *Chem. Mater.* **2007**, *19*, 5063.

[29] J. Chen, X. Wu, A. Selloni, *Phys. Rev. B* **2011**, *83*, 245204.

[30] J. Fester, A. Walton, Z. Li, J. V. Lauritsen, *Phys. Chem. Chem. Phys.* **2017**, *19*, 2425.

[31] J. Fester, M. Bajdich, A. S. Walton, Z. Sun, P. N. Plessow, A. Vojvodic, J. V. Lauritsen, *Top. Catal.* **2017**, *60*, 503.

[32] A. S. Walton, J. Fester, M. Bajdich, M. A. Arman, J. Osiecki, J. Knudsen, A. Vojvodic, J. V. Lauritsen, *ACS Nano* **2015**, *9*, 2445.

[33] S. Kawai, S. Nakatsuka, T. Hatakeyama, R. Pawlak, T. Meier, J. Tracey, E. Meyer, A. S. Foster, *Sci. Adv.* **2018**, *4*, 7181.

[34] N. A. Khan, C. Matranga, *Surf. Sci.* **2008**, *602*, 932.

[35] A. Shiotari, B. H. Liu, S. Jaekel, L. Grill, S. Shaikhutdinov, H.-J. Freund, M. Wolf, T. Kumagai, *J. Phys. Chem. C* **2014**, *118*, 27428.

[36] A. J. U. Holt, S. Pakdel, J. Rodríguez-Fernández, Y. Zhang, D. Curcio, Z. Sun, P. Lacovig, Y.-X. Yao, J. V. Lauritsen, S. Lizzit,

N. Lanatà, P. Hofmann, M. Bianchi, C. E. Sanders, *2D Mater.* **2021**, *8*, 035050.
[37] B. S. Yeo, A. T. Bell, *J. Am. Chem. Soc.* **2011**, *133*, 5587.
[38] X. Lu, Y. H. Ng, C. Zhao, *ChemSusChem* **2014**, *7*, 82.
[39] H.-J. Shin, J. Jung, K. Motobayashi, S. Yanagisawa, Y. Morikawa, Y. Kim, M. Kawai, *Nat. Mater.* **2010**, *9*, 442.
[40] C. Franchini, M. Reticcioli, M. Setvin, U. Diebold, *Nat. Rev. Mat.* **2021**, *6*, 560.
[41] E. Pastor, J.-S. Park, L. Steier, S. Kim, M. Grätzel, J. R. Durrant, A. Walsh, A. A. Bakulin, *Nat. Commun.* **2019**, *10*, 3962.
[42] M. Álvarez-Moreno, C. de Graaf, N. López, F. Maseras, J. M. Poblet, C. Bo, *J. Chem. Inf. Model.* **2015**, *55*, 95.